

## THE DIFFERENTIAL HEAT OF ADSORPTION OF CO<sub>2</sub> ON SMALL-PORT SODIUM MORDENITE: A ONE-DIMENSIONAL, QUASI-EQUILIBRIUM ADSORPTION MODEL\*

M. D. SEFCIK AND H. K. YUEN

*Monsanto Company, St. Louis, Missouri 63166 (U.S.A.)*

### ABSTRACT

The adsorption isotherm and the differential heat of adsorption of CO<sub>2</sub> on small-port sodium mordenite have been measured at 30°C over the range 0.02 torr  $\leq p \leq$  1 atm by a simultaneous DTA/TG technique. Quite uncharacteristic of other zeolites, the isotherm is sigmoidal in shape and the differential heat curve displays several pronounced maxima. The results are discussed in terms of a one-dimensional, quasi-equilibrium model which has been developed with the aid of C-13 NMR. The model assumes that both the high and low energy adsorption sites are periodically spaced in the mordenite channel system and adsorption on the low energy sites effectively restricts the translation of the molecules along the one-dimensional array to other more energetic sites. The model explains many of the unusual adsorption features of the differential heat curve.

### INTRODUCTION

The physical adsorption of molecules on surfaces plays an important role in a variety of industrial processes ranging from drying and separations to catalysis. Understanding the nature of the adsorbate-adsorbent interaction provides useful insight into the properties of the adsorbent surface which are generally quite different from the bulk properties of the material. Even for material with high surface area, the surface may comprise only a small fraction of the total matter compared with the bulk. While many diverse techniques have been used to study the surface region of adsorbents, these measurements usually provide little in the way of information about the properties of the surface in its capacity as an adsorbent. We report here the use of two techniques, thermal analysis and carbon-13 nuclear magnetic resonance, which, when taken together, provide the most complete description of the physical adsorption process obtained to date.

---

\* Presented at the 7th North American Thermal Analysis Society Conference, St. Louis, Missouri, September 25-28, 1977.

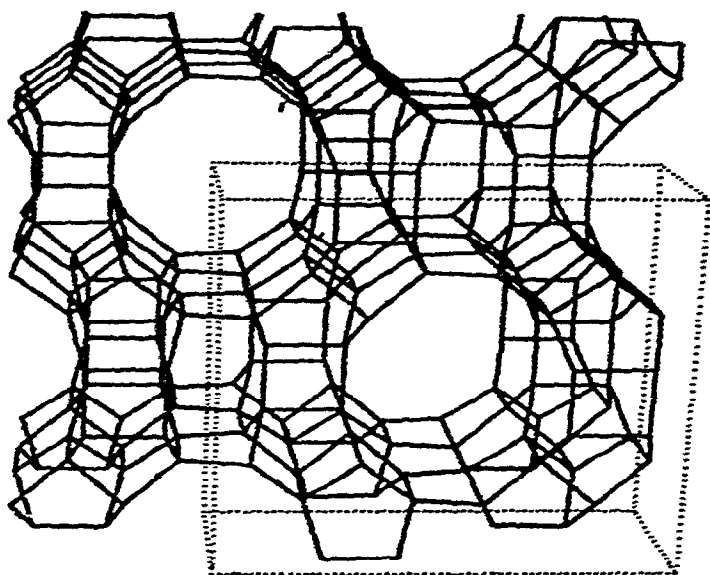


Fig. 1. Mordenite framework; unit cell shown by dotted lines.

#### THE SAMPLE

A sodium mordenite prepared from high purity reagents by L. B. Sand, of Worcester Polytechnic Institute, Worcester, Massachusetts was used in this study. The mordenite has a unit cell formula of  $\text{Na}_8(\text{AlO}_2)_8(\text{SiO}_2)_{40} \cdot 24\text{H}_2\text{O}$  (unit cell dimensions:  $a = 18.13 \text{ \AA}$ ,  $b = 20.49 \text{ \AA}$ ,  $c = 7.52 \text{ \AA}$ )<sup>1</sup> and consists of chains of  $\text{AlO}_4$  and  $\text{SiO}_4$  tetrahedra linked to form 5-rings. The chains of 5-rings are stacked so as to form a two-dimensional channel system as illustrated in Fig. 1. The large channels, which are parallel to the  $c$ -axis, are bound by elliptical 12-rings and have a free aperture of  $6.95 \times 5.81 \text{ \AA}$ . A small-channel system, parallel to the  $a$ -axis, is bound by flat 8-rings (free aperture  $4.72 \times 3.87 \text{ \AA}$ ) and twisted 8-rings (free aperture  $2.8 \text{ \AA}$ ). Rather than interconnecting the large channels, the small-channel system is blocked at the twisted 8-ring by a sodium cation, leaving the large channels lined with side pockets. In addition to the four sodium cations per unit cell which reside in the twisted 8-rings, four other cations are believed to occupy sites scattered in the side pocket itself and in the large channel. Although the large channel dimensions are about  $6 \text{ \AA}$ , some mordenites will not adsorb molecules with a kinetic diameter larger than  $3.8 \text{ \AA}$ . The latter variety, called small-port mordenite, was used in this study.

#### EXPERIMENTAL

##### *Differential heat of adsorption*

The adsorption isotherm and the differential heat of adsorption of  $\text{CO}_2$  by small-port mordenite were measured with the Mettler Thermoanalyzer-1 at  $30^\circ\text{C}$  over a pressure range of  $0.02 \text{ torr} \leq p \leq 1 \text{ atm}$ . The instrument was equipped with a

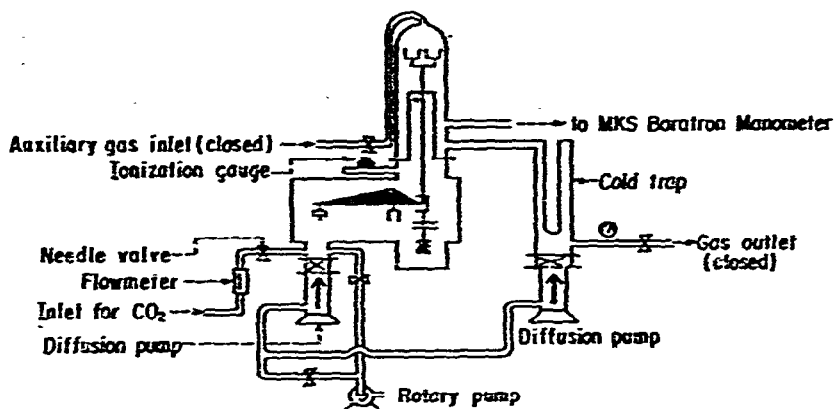


Fig. 2. Schematic drawing of the Mettler TA-1 vacuum system.

differential thermal analysis (DTA) amplifier, thermobalance and high vacuum system. In this experiment, the sample, contained in a 7 mm diameter by 5 mm high cylindrical quartz crucible, was placed on the sample thermocouple of a macro-sample holder. A similar but empty crucible was placed on the reference thermocouple. With the macro-sample holder, the instrument was capable of performing DTA and thermogravimetry (TG) on the same sample simultaneously. This, together with the available high vacuum system made the instrument especially suitable for the adsorption study described herein, since the DTA would monitor the heat due to the adsorption which was quantitatively measured by the TG. To facilitate pressure measurements above 1 torr, the Mettler corrosive gas furnace with auxiliary exit was connected to a MKS Baratron capacitance manometer with a range of 10,000 torr. Pressures below 1 torr were measured with the instrument's thermocouple and ionization gauges. Figure 2 shows a schematic drawing of the experiment.

In order to determine the sample size used for adsorption as accurately as possible, the sample weight was measured *in situ* after the sample was completely degassed. The thermobalance was first calibrated for the 10 mg range used in the experiment in a static  $N_2$  atmosphere. The weight of the macro-sample holder and the two quartz crucibles were then tared on the thermobalance with the standard weights of the balance and the coarse and fine electronic tare adjustments of the instrument. Without changing any settings of the tare, the sample was introduced into its crucible using a Mettler Vibrating Spatula. While at room temperature, the sample and balance chamber were carefully evacuated to a high vacuum with the Balzers rotary pump and two 60 l/sec diffusion pumps of the thermoanalyzer. With the pumps still on, the sample was heated at  $15^\circ\text{C}/\text{min}$  to  $400^\circ\text{C}$ . The sample was considered to be completely degassed when no significant weight loss ( $\Delta w \leq 0.01$  mg in 10 min) was recorded. The ultimate pressure reached at this stage was about  $6 \times 10^{-6}$  torr. The sample was then cooled back to room temperature and the sample and balance were backfilled to 1 atm with dry nitrogen. The thermobalance was again used to determine the equilibrium between the sample and the nitrogen. At equilibrium, the nitrogen flow was shut off and the sample weight determined.

After the sample weight was determined, the sample was evacuated and heated at 15°C/min in a dynamic vacuum to 400°C and cooled at 1°C/min to room temperature. This second degassing was performed to ensure that nitrogen which might have been adsorbed on the sample during weighing was removed.

With an ultimate pressure of  $6 \times 10^{-6}$  torr, the sample was heated at 1°C/min to 30°C where it was held isothermally. The heating rate control was changed to 0.2°C/min for the tightest temperature regulation. When the temperature was stabilized, the diffusion and rotary pumps were shut off and a base weight determined at the system pressure. Dosage of CO<sub>2</sub> required to raise the pressure to the prescribed value was introduced very slowly through the gas inlet needle valve of the instrument into the sample and balance chamber. As adsorption took place, the DTA (with Pt/Pt-10% Rh thermocouples), set at 2 μV/in. sensitivity, recorded an exotherm whose area was proportional to the heat of adsorption. The apparent amount of CO<sub>2</sub> adsorbed was obtained from the weight gain at equilibrium which was being measured simultaneously by the TG. Throughout the experiment, equilibrium was assumed to be attained when no weight change was recorded for 3–4 min and the pressure was the equilibrium pressure in the sample and balance chamber.

#### *Nuclear magnetic resonance*

The carbon-13 nuclear magnetic resonance spectra of isotopically enriched <sup>13</sup>CO<sub>2</sub> were obtained from single resonance experiments which have been described in detail elsewhere<sup>2</sup>. The loading levels of the NMR samples were determined from the equilibrium partial pressure and from the adsorption isotherm.

## RESULTS

#### *Differential heat of adsorption*

To obtain the actual amount of adsorption from the apparent weight gain, it was necessary to correct for the buoyancy effect at each equilibrium pressure. This was achieved by substituting the sample with an approximately equal volume of alumina and repeating the experiment in identical fashion as described above. The buoyancy at the lowest pressure point,  $p = 0.021$  torr, was taken as zero.

The area of the exothermic peak recorded by the DTA at each pressure was measured with a planimeter. In order to determine the proportionality constant which relates the peak area to the amount of heat evolved, the DTA sensitivity was calibrated at each pressure of CO<sub>2</sub> according to

$$\Delta Hm = EA \quad (1)$$

where  $\Delta H$  is the heat of transition in mcal/mg of the standard,  $m$  is the weight (mg) of the standard,  $E$  the proportionality constant at the pressure of interest and  $A$  the area of the DTA peak. Thermometric standards, *p*-nitrotoluene and naphthalene, marketed by Fisher Scientific Company, were used for the calibration. These two standards were chosen because their melting temperatures at 51 and 80°C, respectively, were

closest to the experimental adsorption temperature. The heats of fusion,  $\Delta H_f$  (mcal/mg), of the two standards were first determined in hermetically sealed aluminum pans with a DuPont 990 DSC. Repeated measurements of the standards indicated that their  $\Delta H_f$ 's were reproducible in reheating cycles. Thus, for the Mettler calibration, the same standard was used for the entire pressure range. The sealed standards were placed in the same quartz crucible used to hold the mordenite and another similar but empty aluminum pan was placed in the reference crucible of the DTA. Since the proportionality constant,  $E$ , only depends on temperature and pressure and not heating rate, the standards were heated at  $0.2^\circ\text{C}/\text{min}$  in order to optimize our results due to the poor thermal conductivity of quartz in vacuum. The sensitivity of the DTA and the chart speed of the recorder remained the same as in the adsorption experiment. The  $E$  factors at each pressure obtained for the two standards at their melting temperatures (measured by the extrapolated onset of their respective fusion endotherms) were then extrapolated to  $30^\circ\text{C}$ .

With the proportionality constant known, the adsorption exotherm area was converted to heat by simple multiplication. The result obtained,  $Q_j$ , was the amount of heat due to the adsorption of  $(W_j - W_{j-1})$  mg of  $\text{CO}_2$ , where  $W_j$  and  $W_{j-1}$  were the total amounts of  $\text{CO}_2$  adsorption at the pressures  $j$  and  $j - 1$ , respectively. Since  $(W_j - W_{j-1})$  was equivalent to about  $10^{-4}$  moles of  $\text{CO}_2/\text{g}$  of sample throughout

TABLE 1

$\text{CO}_2$  ADSORPTION ON SODIUM SMALL-PORT MORDENITE AT  $30^\circ\text{C}$

Pressure (Torr)	$Q_D$ (kcal/mole)	Moles of $\text{CO}_2$ adsorbed/g of sample ( $\times 10^4$ )
0.018		1.68
0.046		2.15
0.115		2.76
0.27		2.99
0.55	18.172	3.68
0.90	8.845	5.14
1.90	5.866	10.71
5.10	10.960	16.42
10.10	12.900	19.05
20.10	7.953	21.63
40.2	8.850	24.11
60.2	9.164	25.77
80.5	6.749	26.92
100.0	9.788	27.94
150.3	8.753	29.52
200.1	6.586	31.03
400.2	6.601	34.83
741.3	7.791	38.99

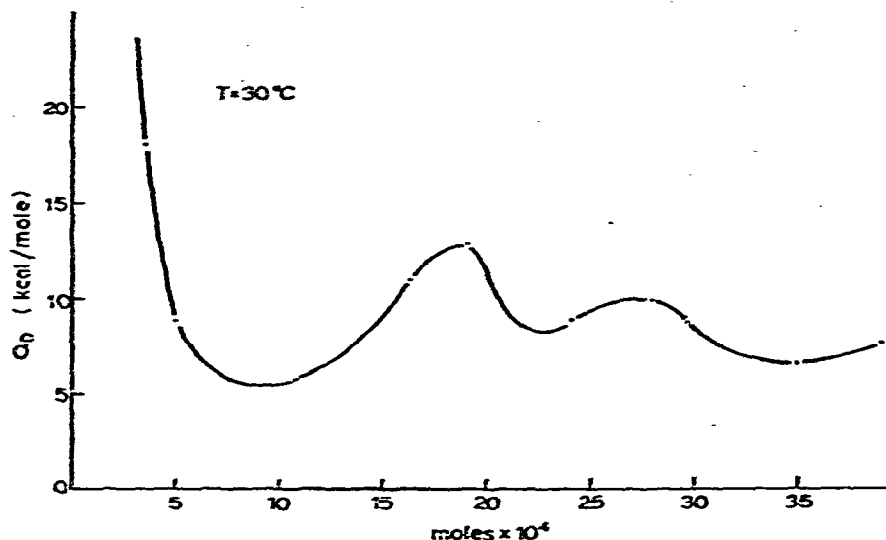
differential heat of adsorption of CO<sub>2</sub>

Fig. 3. Differential heat of adsorption of CO<sub>2</sub> on small-pore sodium mordenite at 30°C.

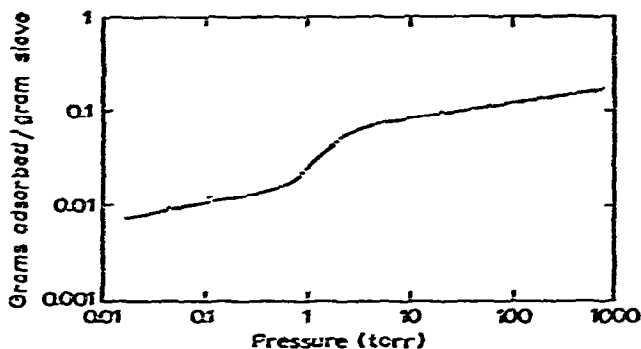


Fig. 4. Adsorption isotherm of CO<sub>2</sub> on small-pore sodium mordenite at 30°C.

the entire pressure range, the differential heat of adsorption at pressure  $j$  could be approximated by

$$Q_{D,j} = \frac{Q_j}{\Delta n} = \frac{Q_j}{(W_j - W_{j-1})} \times 10^3 \times 44 \quad (2)$$

Table I shows the adsorption results obtained. In Fig. 3, the differential heat of adsorption,  $Q_D$  (kcal/mole) is plotted versus the number of moles of CO<sub>2</sub> adsorbed/g of mordenite. Figure 4 shows the adsorption isotherm for CO<sub>2</sub> at 30°C.

#### Nuclear magnetic resonance

Previous results on the <sup>13</sup>C-NMR of CO<sub>2</sub> adsorbed on the small-pore mordenite indicated that at low coverages the CO<sub>2</sub> molecules were nonrotating while at high coverages they behaved as anisotropic rotors<sup>2</sup>. The nonrotating molecules were

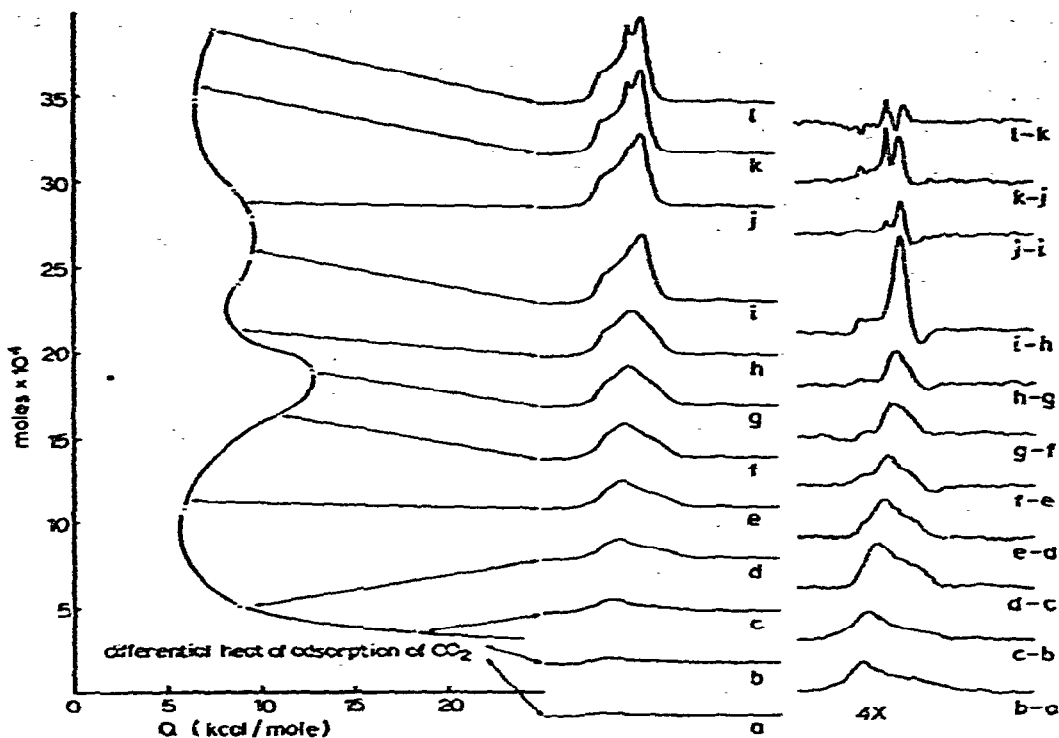


Fig. 5.  $^{13}\text{C}$ -NMR spectra of  $\text{CO}_2$  adsorbed on small-pore sodium mordenite: spectra (a) through (l), variation in NMR spectra with coverage; spectra (b-a) through (l-k), difference spectra.

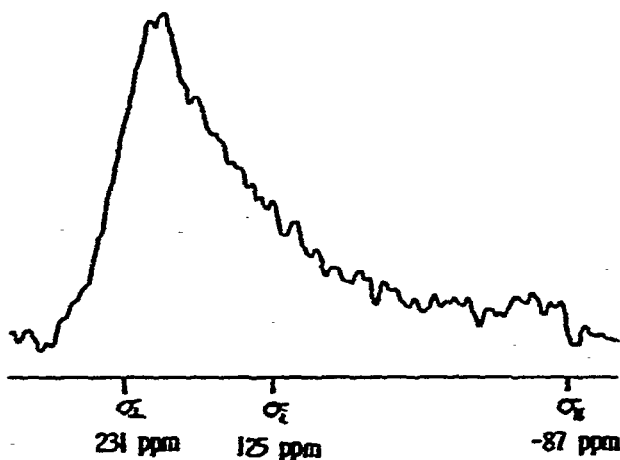


Fig. 6.  $^{13}\text{C}$ -NMR spectrum of  $1.9 \times 10^{-4}$  moles/g of  $\text{CO}_2$  adsorbed on small-pore sodium mordenite. The chemical shift dispersion is that of an axially symmetric nonrotor with its isotropic center ( $\sigma_0$ ) at 125 ppm relative to TMS.  $\sigma_1$  and  $\sigma_{11}$  are the perpendicular and parallel components of the chemical shift tensor.

assumed to be adsorbed in the side pockets which line the large channel while adsorption in the large channel itself led to both nonrotating and anisotropic rotating adsorbed molecules. Although some molecules were observed to rotate isotropically, it was felt that this was due to adsorption in the macrostructure on the surface of the

zeolite crystal. We present here a more detailed study of the NMR spectra of adsorbed  $\text{CO}_2$  which has been extended to much lower coverages.

The nuclear magnetic resonance spectra of adsorbed  $\text{CO}_2$  are presented in the center of Fig. 5 (a)–(l). At the lowest loading level studied here,  $1.9 \times 10^{-4}$  moles/g, the NMR spectrum displays a chemical shift dispersion of a nonrotating, axially symmetric molecule. This spectrum is shown on an expanded scale in Fig. 6. The separation between the chemical shift tensors is estimated to be  $318 \pm 18$  ppm, agreeing remarkably well with the calculated value of 315 ppm for  $^{13}\text{CO}_2$  in a perfectly rigid matrix<sup>3</sup>.

Upon increasing the coverage to  $2.7 \times 10^{-4}$  moles/g, the  $^{13}\text{CO}_2$  resonance can be seen to narrow slightly [Fig. 5(b)]. A somewhat more informative way to view the changes in the NMR spectrum due to the increased coverage can be obtained by subtracting the spectrum obtained at the lower loading level from that at the higher level resulting in a difference spectrum. The difference spectrum, Figure 5(b-a) corresponds to the NMR spectrum of the  $8 \times 10^{-5}$  moles of  $\text{CO}_2/\text{g}$  which were adsorbed on the mordenite between obtaining the spectra 5(a) and 5(b). The major component of this spectrum has a chemical shift dispersion of about 265 ppm, somewhat less than expected for rigid  $\text{CO}_2$  molecules. In the successive difference spectra, Figs. 5(c-b), 5(d-c) and 5(e-d), the NMR linewidth decreases to 175, 140 and 105 ppm, while retaining the chemical shift dispersion of a relatively rigid axially symmetric molecule.

Beginning with Fig. 5(f), at a loading level of  $1.6 \times 10^{-3}$  moles/g, the chemical shift dispersions take on the characteristic shape of an axially symmetric rotor, that is, the most intense portion of the resonance shifts from the low field to the high field side of the spectrum<sup>4</sup>. This trend continues to become more pronounced as the loading level is increased towards saturation. Near saturation, a narrow line component of the spectra can be seen located at the isotropic center of the chemical shift dispersion.

The difference spectra from two regions of the coverage range examined here are unique from the others. In the coverage range of about 0.5–1.6 and  $1.9\text{--}2.8 \times 10^{-3}$  moles/g, the difference spectra displays regions of negative area (the baseline is taken as zero) indicating a loss of spectral density upon adsorption of additional  $\text{CO}_2$ . In fact, however, the areas in all of the spectra are proportional to the coverage indicated by the adsorption isotherm so we may conclude that all of the adsorbed molecules were observed. The loss of spectral density can only be accounted for as a rearrangement in the chemical shift dispersion of the adsorbed molecules caused by the addition of more molecules. That is, the rotational behavior of some adsorbed molecules is altered by the adsorption of additional molecules.

#### DISCUSSION

The differential heat of adsorption of  $\text{CO}_2$  on the small-pore sodium mordenite displays several pronounced maxima, suggesting a very heterogeneous adsorption process. The initial very high heat of adsorption is expected as the first molecules become situated on the most energetic adsorption sites and  $Q_D$  steadily decreases due

to the successive filling of less energetic sites. The presence of maxima in the differential heat of adsorption curve, however, is quite unusual, having only been observed for the adsorption of carbon dioxide on mordenite<sup>5</sup> and chabazite<sup>6</sup>.

Some features of the differential heat curve can be rationalized by examining the energetics of the various interactions which occur upon adsorption while utilizing the nuclear magnetic resonance results to identify the location of the site and the behavior of the adsorbed molecules.

The initial heat of adsorption, which has been well studied<sup>7</sup>, depends on the dispersion and repulsion energies which arise as the CO<sub>2</sub> approaches the surface as well as the energies which are due to the interaction between the electrostatic fields of the zeolite and the adsorbate. The initial heat of adsorption of CO<sub>2</sub>, which does not contain a permanent dipole, is given by

$$\Delta H_i = \phi_D + \phi_R + \phi_P + \phi_{F-Q} \quad (3)$$

where the dispersion and short-range repulsion energies are given by a Lennard-Jones potential

$$\phi_D = - \frac{A}{r^6} \quad (4)$$

$$\phi_R = \frac{B}{r^{12}} \quad (5)$$

where the constants  $A$  and  $B$  are determined by the lattice structure and the adsorbate and  $r$  is the equilibrium separation distance. The polarization term,  $\phi_P$ , is given by

$$\phi_P = - \frac{\alpha F^2}{2} \quad (6)$$

where  $\alpha$  is the polarizability of the adsorbate and  $F$  the field strength. The interaction between the cation field gradient and the electric quadrupole moment of the adsorbate,  $\phi_{F-Q}$ , is

$$\phi_{F-Q} = - \frac{QF}{4r} (3 \cos^2 \theta - 1) \quad (7)$$

where  $Q$  is the electric quadrupole moment and  $\theta$  is the angle between the axes of the quadrupole and the field gradient.

As the concentration of molecules adsorbed on the surface increases, one must also account for interactions between adsorbates. Thus, the heat of adsorption at higher loading levels will be determined by the dispersion energy and quadrupole-quadrupole effects for CO<sub>2</sub>-CO<sub>2</sub> interactions as well as the CO<sub>2</sub>-surface interactions [eqn. (3)].

$$\Delta H = \Delta H_i + \phi + \phi_{QQ} \quad (8)$$

The mutual interaction between CO<sub>2</sub> molecules may be described by the potential

$$\phi = 4\epsilon \left[ \left( \frac{r_0}{r} \right)^{12} - \left( \frac{r_0}{r} \right)^6 \right] \quad (9)$$

where  $\epsilon$  and  $r_0$  are obtained from the second virial coefficients using the Lennard-Jones potential<sup>8</sup>. The interactions between the quadrupole is given by<sup>6</sup>

$$\phi_{QQ} = \frac{3Q^2}{16r^5} [1 - 5\cos^2\theta_1 - 5\cos^2\theta_2 + 17\cos^2\theta_1\cos^2\theta_2 + \\ + 16\sin\theta_1\cos\theta_1\sin\theta_2\cos\theta_2\cos(\phi_1 - \phi_2) + 2\sin^2\theta_1\sin^2\theta_2\cos^2(\phi_1 - \phi_2)] \quad (10)$$

where  $\theta_1$  and  $\theta_2$  are the angles between the quadrupole axes and the line joining their centers and  $(\phi_1 - \phi_2)$  is the angle between the planes formed by the quadrupole axes and the line joining their centers.

In the region of low coverage, ( $5 \times 10^{-4}$  moles/g) where the differential heat of adsorption decays smoothly, we can describe the interaction energetics by eqn. (3). The structure of the mordenite would suggest the presence of two adsorption sites, a very energetic site in the side pockets which line the large channel and less energetic sites in the large channel itself. If we assume that the adsorption is an equilibrium process, then the sites will be filled in accord with their energy distribution as dictated by the Boltzmann function. Thus, at low coverage, we expect that the energetic side-pocket sites will be filled first. The observed decrease in the heat of adsorption would then represent the energy distribution of the side-pocket adsorption sites.

As expected, the NMR spectra indicate that each successive charge of molecules is adsorbed into sites which offer greater rotational freedom and hence, as predicted by eqn. (3), must have lower heats of adsorption. Since the NMR linewidth of the chemical shift dispersion is proportional to the square of the cosine of the angle of

TABLE 2

VARIOUS CONTRIBUTIONS TO THE HEAT OF ADSORPTION

$n \times 10^4$ moles/g	Line- width ppm	$\theta$ radians	$r_{max}$ $\text{\AA}$	$Q_D^a$ (kcal/mole)	$\phi_{\bar{r}-0}^b$ (kcal/mole)	$Q_D$ (kcal/mole)
1.9	318	$\sim 0$	$\sim 2.8$	$\sim -66$	$\sim -5.1$	
2.7	265	0.41	3.26	-26.6	-4.8	
3.7	175	0.73	3.57	-15.4	-4.0	-18.0
5.0	140	0.84	3.66	-13.2	-3.6	- 8.5
11.0	105	0.95	3.75	-11.5	-3.1	- 5.8

<sup>a</sup>  $\alpha_{CO_2} = 4.1 \times 10^{-24}$  cm<sup>3</sup>/particle;  $\alpha_0 = 1.65 \times 10^{-24}$  cm<sup>3</sup>/particle;  $X_{CO_2} = -30.9 \times 10^{-29}$ ;  $X_0 = -20.9 \times 10^{-29}$ .

<sup>b</sup> Assuming  $-\frac{QF}{4r}(3\cos^2\theta - 1) = -5.1$  when  $\theta = 0$ .

rotation, it is possible to estimate the average rotational freedom of the adsorbed molecules from the difference spectra of Fig. 5. Given in Table 2 are the NMR linewidths at various coverages and the angle of rotational freedom,  $\theta$ , calculated from eqn. (11).

$$\frac{\text{motional averaged linewidth}}{\text{rigid linewidth}} = \cos^2 \theta \quad (11)$$

Since the rotation of the adsorbed  $\text{CO}_2$  molecule is presumably restricted by repulsive interactions with the adsorption site walls, an average distance between the center of the  $\text{CO}_2$  and the center of the surrounding lattice oxygens can be calculated from  $\theta$ , the O-O distance and the van der Waals radii for  $\text{CO}_2$  molecule. (Use of the van der Waals radii rather than the Lennard-Jones or kinetic radii is justified here since the latter are derived for isotropically rotating molecules).

With an estimate of the average distance between the adsorbed molecule and the cavity walls,  $r_{\text{max}}$ , it is possible to estimate the dispersion energy from eqn. (4) by choosing an appropriate description for the adsorption site. In the case of side-pocket adsorption, the site can be approximated by a cylindrical pore whose radius to the center of the surrounding lattice oxygen atom is given by  $r_{\text{max}}$  and has a depth of 5 Å as determined from crystallographic measurements. It is also assumed that a net charge of one cation resides at the closed end of the pore. The dispersion energy listed in Table 2 was calculated from eqn. (4) where  $A$  is given by the Kirkwood-Muller expression<sup>9</sup>

$$A = 6 mc^2 \left( \frac{\alpha_1 \alpha_2}{\frac{\alpha_1}{X_1} + \frac{\alpha_2}{X_2}} \right) \quad (12)$$

where  $m$  is the mass of an electron,  $c$  the velocity of light, and  $\alpha$  and  $X$  are the polarizability and diamagnetic susceptibility of the adsorbate-oxygen pair. To simplify the calculation, it was assumed that each of the twenty lattice oxygens which form the adsorption pore are equivalent and equally spaced from the  $\text{CO}_2$ . An additional eight second-nearest neighbors were not included in the calculation.

The contribution to the heat of adsorption from the field-gradient quadrupole interaction listed in Table 2 was determined by first calculating the relative change in  $\phi_{\text{F-Q}}$  due to the angle dependence of eqn. (7). The value of  $\phi_{\text{F-Q}}$  for a  $\text{CO}_2$  molecule in intimate contact with a sodium cation in zeolite-X has been calculated by Barrer and Gibbons<sup>10</sup> to be  $-5.1$  kcal/mole. The field-gradient quadrupole interaction for  $\text{CO}_2$  on sodium large-port mordenite has been estimated<sup>7</sup> to be  $-9$  kcal/mole based on a comparison of the isosteric heat of adsorption of the  $\text{Na}^+$  and  $\text{H}^+$  forms of mordenite. We believe, however, that the latter value is erroneously high since  $\text{CO}_2$  molecules are not adsorbed into the same sites on these two mordenites<sup>2</sup>. For this work, the value of  $-5.1$  kcal/mole for  $\phi_{\text{F-Q}}$  was chosen for the heat of adsorption when  $\theta = 0$ .

Other contributions to the initial heat of adsorption due to repulsion and

polarization have not been considered here. We have assumed that the repulsion energy is infinite when the separation is less than the van der Waals radii and zero when it is greater. The variation in polarization energy is assumed to be small. The maximum polarization energy for CO<sub>2</sub> adsorbed on sodium zeolite-X has been calculated<sup>10</sup> to be  $-1.2$  kcal/mole. We have also ignored the influence of a filled adsorption site on the energetics of the neighboring adsorption site. In fact, eight of the twenty lattice oxygens which form the side pocket are shared, four each, with the two adjoining side pockets. However, since nearly one-half of the adsorption capacity of the mordenite is in the side pockets, adjoining side pockets need not be filled at low coverage.

From the results of Table 2 it is clear that the initial decrease in the heat of adsorption is consistent with a dispersion of interaction energies due to slight variations in the dimensions of the side-pocket adsorption site. It is also clear, however, that the equilibrium adsorption model does not account for as great a decrease in the differential heat of adsorption as was observed nor is it consistent with the occurrence of a maximum in the heat of adsorption at increased coverage.

The failure of the equilibrium model to describe the adsorptive process can be seen from the following argument. If the system is at equilibrium, then at the coverage of  $1.1 \times 10^{-3}$  moles/g all of the adsorption sites which are more exothermic than the observed differential heat of  $\sim 6$  kcal/mole must be filled. If this is the case, then the maximum in the differential heat curve which appears at about  $2 \times 10^{-3}$  moles/g must be due to contributions from the adsorbate-adsorbent interactions (of not more than 6 kcal/mole) and from adsorbate-adsorbate interactions as has been suggested by other authors<sup>5, 6</sup>. An estimate of the mutual interaction energy for a pair of CO<sub>2</sub> molecules can be obtained from eqns. (9) and (10). Using the Lennard-Jones parameters of Danon and Pitzer<sup>11</sup> which include the quadrupole effect, the maximum dispersion energy is  $-535$  cal/mole. At the equilibrium separation of 3.85 Å determined by the above authors, the maximum quadrupole-quadrupole interaction<sup>6</sup> is  $-505$  cal/mole for a total mutual interaction energy of about 1.04 kcal/mole. Thus, we can account for only about 7 of the 12.5 kcal/mole at the maximum using this model.

Measurements of the differential heat of adsorption on large-pore sodium and hydrogen mordenite<sup>5</sup> indicate the intensity of the maximum increases with increasing temperature and occurs at lower loading levels. These results also seem to be inconsistent with the concept of adsorbate-adsorbate interactions as the cause of the differential heat maximum. The failure of this model can be attributed to the assumption that the adsorbed molecules are at a true equilibrium and have equal access to both the high energy side-pocket sites and the lower energy sites in the main channel.

The maximum in the differential heat curve is more easily explained by a one-dimensional, quasi-equilibrium model in which both high and low energy adsorption sites are spaced periodically in the mordenite channel system. We can then assume that molecules will be distributed between side pocket (high energy) and channel (low energy) sites and the gas phase, depending on their energy separation.

However, the distribution will not be Boltzmann, since the one-dimensionality of the channel system does not allow equal access to each adsorption site except in the limit of zero coverage. In this limit, adsorption will occur predominantly in the side pockets near the opening of the channel system. At slightly higher coverage, the gas molecules entering the mordenite channel system will encounter only a series of low energy potential wells as the high energy sites have already been filled. Depending on the length of the channel which the adsorbate must traverse to find an empty side pocket and the difference in energy levels, there is a finite probability that adsorption will occur in the low energy channel sites.

The consequence of this model is that, after a period of adsorption into the high energy side-pocket sites, some molecules will adsorb in the channel sites and effectively restrict further translation of molecules to the other energy-rich sites, creating a quasi-equilibrium state. This state is characterized by the fact that all of the adsorbed molecules are in the lowest energy states to which they have access, but there is a large number of very energetic sites which are not filled. To this point, the differential heat of adsorption shows a systematic decrease with coverage reflecting the adsorption site heterogeneity described above. However, as a function of either temperature or pressure, the chemical potential of the gas molecules increases. This reduces the potential barrier and allows free translation. When free translation occurs, the gas molecules have easy access to the high energy side-pocket sites and very exothermic adsorption is observed. Thus, the presence of a few molecules adsorbed in the large-channel sites provides a potential energy barrier to free translation which must be overcome by temperature or pressure of the gas molecules.

This model successfully explains both the position and the intensity of the maximum in the differential heat of adsorption of  $\text{CO}_2$  on mordenite which were observed by ourselves and other authors<sup>5</sup>. Further verification that the maximum occurs after the onset of free translation in the large channel is obtained from the NMR spectra. As noted above, the difference NMR spectrum corresponding to the initial rise in the differential heat maximum, Fig. 5(f-e), not only shows that newly adsorbed molecules are anisotropically rotating, but that some molecules which were previously nonrotors have also been induced to anisotropically rotate. A consequence of the anisotropic rotation is that the quadrupole interaction is reduced by a factor of four [see eqn. (5)] and the dispersion energy is decreased due to the greater average distance between the rotating molecule and the surface. Since anisotropic rotation is not possible in the side pockets, we must conclude that we are observing the change in behavior of molecules which are blocking the large channel. These results suggest a decrease in the potential energy barrier in the large channel and greater mobility of the adsorbed molecules. Sharp transitions between bound and freely translating molecules as a function of temperature have been observed by other authors<sup>12, 13</sup>.

The exact origin of the second maximum in the differential heat curve cannot be deduced from our results with certainty. The difference NMR spectra in this region, which indicate also a transition from bound to anisotropically rotating molecules, suggest that it may arise in a similar fashion as the first maximum. However, with the

intensity of this second maximum only on the order of the  $\text{CO}_2$ - $\text{CO}_2$  mutual interaction energy, it is felt that, until further experimental evidences could be established, any conclusion on its real cause would be premature.

#### CONCLUSION

With the aid of the differential heat of adsorption and the NMR spectra for adsorbed carbon dioxide, a one-dimensional, quasi-equilibrium adsorption model has been developed. The model successfully accounts for the features of both experiments and provides a basis for understanding the kinetics of catalytic reaction on molecular sieves with one-dimensional channel systems.

#### REFERENCES

- 1 W. M. Meier, *Z. Kristallogr.*, 115 (1961) 439.
- 2 M. D. Sefcik, Jacob Schaefer and E. O. Stejskal, *Molecular Sieves-II*, *ACS Symp. Ser.*, 40 (1977) 344.
- 3 H. W. Siess, D. Schweitzer, U. Haebleren and K. H. Hausser, *J. Magn. Reson.*, 5 (1971) 101.
- 4 All of the NMR spectra presented here are displayed with the field strength increasing from left to right.
- 5 P. Cartaud, *Thermochim. Acta*, 16 (1976) 197.
- 6 G. L. Kingston and A. C. Macleod, *Trans. Faraday Soc.*, 51 (1959) 1799.
- 7 R. M. Barrer, *J. Colloid Interface Sci.*, 21 (1966) 415.
- 8 J. A. Pople, *Proc. Roy. Soc. London, Ser. A*, 221 (1954) 508.
- 9 J. G. Kirkwood, *Phys. Z.*, 33 (1932) 57; A. Muller, *Proc. Roy. Soc. London, Ser. A*, 154 (1936) 624.
- 10 R. M. Barrer and R. M. Gibbons, *Trans. Faraday Soc.*, 61 (1965) 948.
- 11 F. Danon and K. S. Pitzer, *J. Chem. Phys.*, 36 (1962) 425.
- 12 T. Takaishi, A. Yusa, Y. Ogino and S. Ozawa, *Trans. Faraday Soc.*, 70 (1974) 671.
- 13 R. M. Barrer and W. I. Stuart, *Proc. Roy. Soc. London, Ser. A*, 249 (1959) 484.